Superconducting properties of the noncentrosymmetric superconductor LaPtGe

Sajilesh K. P.,[1] D. Singh,[1] P. K. Biswas,[2] A. D. Hillier,[2] and R. P. Singh[1,*]

[1]*Department of Physics, Indian Institute of Science Education and Research Bhopal, Bhopal 462066, India*
[2]*ISIS Facility, STFC Rutherford Appleton Laboratory, Harwell Science and Innovation Campus, Oxfordshire OX11 0QX, United Kingdom*

We report on the superconducting properties of noncentrosymmetric superconductor LaPtGe, which crystallizes in noncentrosymmetric α-ThSi$_2$ structure. The magnetization, resistivity, and specific-heat measurements confirm that LaPtGe is a type-II bulk superconductor with a transition temperature $T_c = 3.05 \pm 0.05$ K. Muon-spin relaxation/rotation measurements suggest that time-reversal symmetry is preserved in the superconducting ground state.

I. INTRODUCTION

In recent years, several new superconducting materials have been discovered. Many of these new superconductors are described as "unconventional," as their superconducting properties deviate from traditional BCS theory [1]. Noncentrosymmetric superconductors (NCSs) have emerged as an exciting class of new unconventional superconductors. The lack of inversion symmetry can make the pairing scenario different, which introduces the possibility of a vast array of exotic physics [2–5]. A nontrivial antisymmetric spin-orbit coupling (ASOC) that arises due to an asymmetric electric-field gradient lifts the original conduction electron spin degeneracy at the Fermi level, splitting it into two sublevels [6]. This leads to an admix superconducting ground state that exhibits many exotic properties that have not been observed in conventional superconductors [7–15]. The admixed pairing state can be manipulated by tuning the ASOC, which directly controls the mixing ratio of the singlet/triplet pairing channel [16]. In addition, the importance of electronic correlations, which often facilitate the interaction between different pairing channels, cannot be neglected. Strongly correlated superconductors without inversion symmetry include CePt$_3$Si [17], Re$_6$ (Zr,Hf,Ti) [18–23], and UIr [24], while LaNiC$_2$ [25], Li$_2$$M_3$B ($M$ = Pd, Pt) [16,26], and La$_7$Ir$_3$ [27] are weakly correlated. Weakly correlated materials are of great importance since the effects of broken inversion symmetry and asymmetric spin-orbit coupling interactions can be more explicitly separated and understood.

At present, the major issue in this area is how the antisymmetric spin-orbit coupling influences the parity mixing in these materials and the presence/absence of time-reversal symmetry breaking (TRSB). Until now, only a small number of superconductors have been discovered that exhibit TRSB [18,25,27–32], which makes it difficult to determine the roles of asymmetric spin-orbit coupling and electron correlations in noncentrosymmetric superconductors. Therefore, it is crucial to search for new superconductors whose crystal structure lacks inversion symmetry.

In this paper, we report on a comprehensive study of the superconducting properties of the noncentrosymmetric ternary equiatomic compound LaPtGe, which is a ternary variant of α-ThSi$_2$ structure in which a three-dimensional network of three connected metalloid atoms is found with tetragonal symmetry [33]. Theoretical calculations on the ternary variant of the α-ThSi$_2$ compounds show strong spin-orbital coupling strength [34]. The calculation of Kneidinger *et al.* on the parent ternary compound LaPtSi revealed strong ASOC [35]. It is interesting to look for more compounds in the same family to find the effect of ASOC on the superconducting ground state, in particular LaPtGe in the present case. Here we have used resistivity, magnetization, and heat capacity along with muon-spin spectroscopy to probe the gap symmetry and nature of the superconducting ground state.

II. EXPERIMENTAL DETAILS

Polycrystalline LaPtGe samples were prepared using a standard arc-melting technique. High-purity La (99.99%), Pt (99.99%), and Ge (99.99%) were taken in a stoichiometric ratio and melted in a water-cooled copper hearth under high-purity argon gas. The resulting ingot formed with the negligible mass loss was flipped and remelted several times to improve the homogeneity. The phase purity and crystal structure of the sample were confirmed by room-temperature x-ray diffraction measurement using a PANalytical diffractometer equipped with Cu $K\alpha$ radiation ($\lambda = 1.5406$ Å). Magnetization measurements were done using a superconducting quantum interference device (MPMS 3, Quantum Design). The electrical resistivity and heat-capacity measurements of the sample were performed using a Physical Property Measurement System (PPMS, Quantum Design). The μSR experiments were carried out using a 100% spin-polarized pulse muon beam at ISIS facility, Rutherford Appleton Laboratory, Didcot, United Kingdom.

III. RESULTS AND DISCUSSION

A. Sample characterization

The x-ray diffraction pattern is shown in Fig. 1. Rietveld refinement to the data was done using FULLPROF
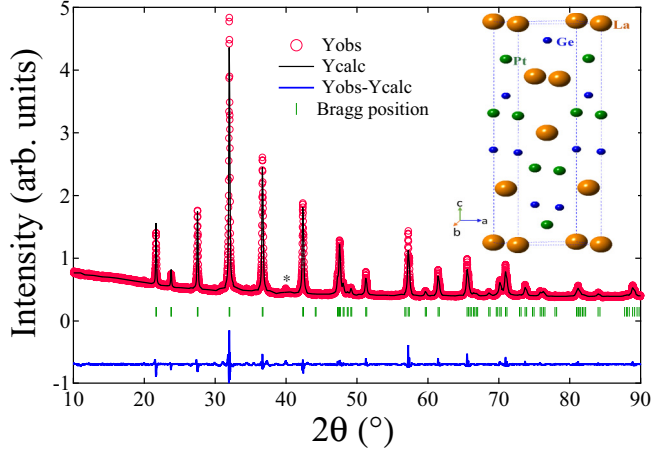
*rpsingh@iiserb.ac.in

FIG. 1. Powder x-ray diffraction pattern for the LaPtGe sample obtained at room temperature using Cu $K\alpha$ radiation (red line). The solid black line shows the Rietveld refinement. The inset shows the crystal structure of LaPtGe.

FIG. 2. Temperature dependence of resistivity in the range $1.8 \leqslant T \leqslant 300$ K. The inset shows the drop in resistivity at the superconducting transition, $T_C = 3.05 \pm 0.03$ K. The normal-state resistivity is fitted with the parallel-resistor model in the temperature range $5 \leqslant T \leqslant 300$ K.

software, which shows that the sample crystallizes into a tetragonal, noncentrosymmetric structure (space group $I4_1md$) with derived lattice parameters $a = b = 4.2655(2)$ Å, $c = 14.9654(1)$ Å. The lattice parameters obtained in this work are in good agreement with data reported previously [33]. A small impurity peak is observed around $40°$ (denoted by an asterisk) due to Pt_3Ge. Any significant effect of this impurity phase is not observed in bulk and muon spectroscopy measurements. The inset in Fig. 1 shows the crystal structure of LaPtGe.

B. Normal and superconducting state properties

1. Electrical resistivity

The temperature dependence of the electrical resistivity $\rho(T)$ of LaPtGe in the temperature range 1.8–300 K in zero applied magnetic field is shown in Fig. 2. A characteristic drop in resistivity, observed at $T_C = 3.05 \pm 0.03$ K, is shown in the inset of Fig. 2. The residual resistivity ratio is comparable to other LaNiSi structure compounds [35]. A high value of absolute resistivity with the saturation behavior at high temperatures indicates that the data can well be described by the parallel-resistor model [36]. The saturation at high temperatures typically happens when the apparent mean free path becomes short, of the order of a few interatomic spacings [37,38]. In such a scenario, the scattering cross section will not be linear in scattering perturbation. At high temperatures, the dominant temperature-dependent scattering mechanism is the electron-phonon interaction. So the resistivity will not be proportional to the mean-square atomic displacement, which is proportional to T for the harmonic potential. Instead, it will rise less rapidly with T showing a saturating behavior. In general, the electrical resistivity of a metal, for $T > T_C$, can be written as [36,39]

$$\rho_i(T) = \rho_{i,0} + \rho_{i,L}(T). \tag{1}$$

In this relation, the temperature-independent residual resistivity, which arises from impurities and disorder, is denoted by $\rho_{i,0}$, while the second term adds the temperature-dependent
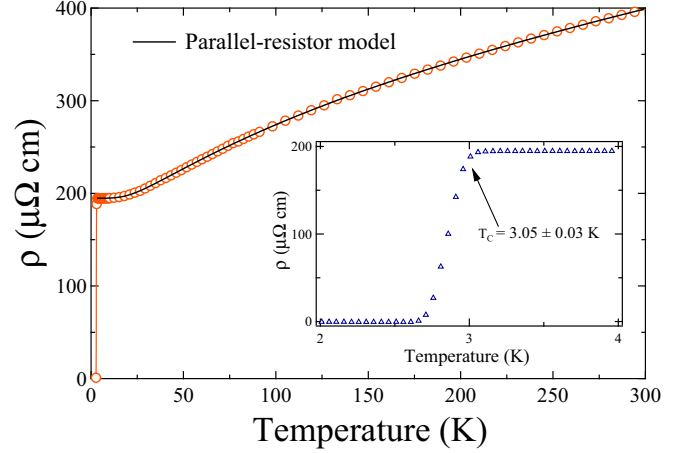
general resistivity, which can be written according to the generalized Bloch-Grüneisen expression [40]

$$\rho_{i,L}(T) = C\left(\frac{T}{\Theta_D}\right)^5 \int_0^{\Theta_D/T} \frac{x^5}{(e^x - 1)(1 - e^{-1})} dx, \tag{2}$$

where Θ_D is the Debye temperature obtained from resistivity measurements, while C is a material-dependent prefactor. In the case of saturation resistivity, the resistivity curve, considering the saturation at high temperature can be explained by

$$\rho(T) = \left[\frac{1}{\rho_s} + \frac{1}{\rho_i(T)}\right]^{-1}, \tag{3}$$

where ρ_s is the temperature-independent saturation value of resistivity, which will be attained at high temperatures.

A fit employing this model is shown in Fig. 2, and it yields a Debye temperature $\Theta_D = 139 \pm 3$ K, $C = 936 \pm 7$ $\mu\Omega$ cm, residual resistivity $\rho_{i,0} = 253 \pm 2$ $\mu\Omega$ cm, $\rho_s = 848 \pm 4 \mu\Omega$ cm. The values of the fit parameters are similar to those obtained for other intermetallic samples [39].

2. Magnetization

Figure 3(a) shows the dc susceptibility data taken in an applied field of 2 mT in zero-field-cooled (ZFC) and field-cooled-cooling (FCC) modes. Superconductivity defined as the onset of the diamagnetization signal appears at $T_c^{onset} = 3.05 \pm 0.05$ K. The Meissner fraction value exceeds 100% due to the uncorrected geometrical demagnetization factor. The temperature-independent paramagnetic behavior for $T > T_C$ suggests the absence of any magnetic impurities in the sample. The low-field magnetization measurement as a function of applied magnetic field (0–10 mT) is taken at different temperatures to calculate the lower critical field H_{C1} [see the inset in Fig. 3(b)]. The first deviation from linearity from the initial slope is taken as the basis to determine H_{C1} for all the respective temperatures. Figure 3(b) depicts the resulting temperature dependence of H_{C1}, which is fitted by
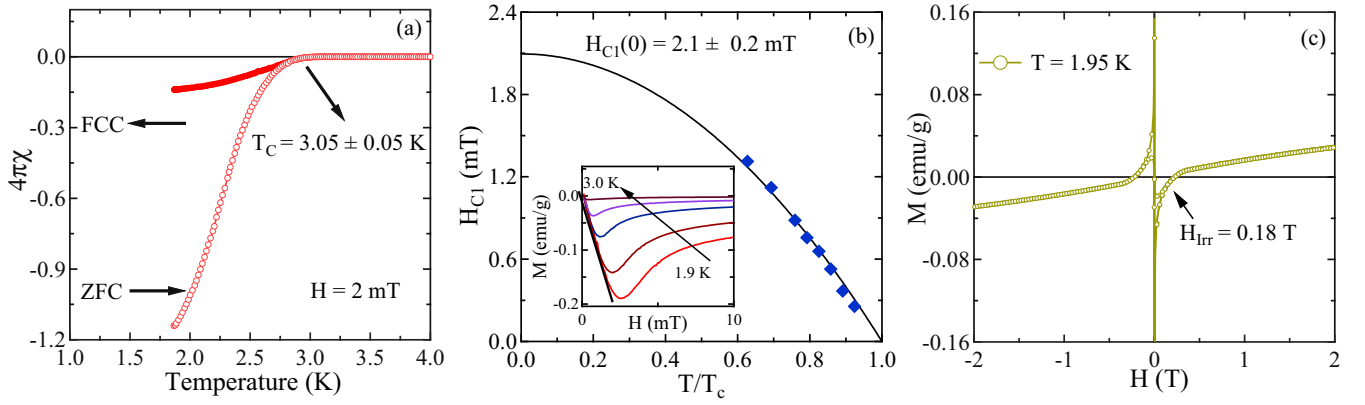
FIG. 3. (a) Temperature dependence of the magnetic moment collected via zero-field-cooled warming (ZFC) and field-cooled-cooling (FCC) methods under an applied field of 2 mT. (b) Temperature dependence of lower critical field H_{C1}. The inset shows the low-field magnetization data at different temperatures. (c) Magnetization data collected at 1.95 K in the range $-2 \leqslant H \leqslant +2$ T showing an irreversible field $H_{\mathrm{irr}} = 0.18$ mT.

the Ginzburg-Landau equation

$$H_{C1}(T) = H_{C1}(0)\left[1 - \left(\frac{T}{T_C}\right)^2\right]. \quad (4)$$

The value of $H_{C1}(0)$ was estimated to be 2.1 ± 0.2 mT after fitting Eq. (4) in the $H_{C1}(T)$ plot. Figure 3(c) presents the high-field magnetization loop collected at 1.95 K in the magnetic-field range ± 2 T. The magnetic behavior exhibits conventional type-II superconductivity with an irreversible nature of magnetization below $H_{\mathrm{irr}} = 0.18$ mT, above which point the applied field becomes strong enough to depin the vortices.

To measure the upper critical field as a function of temperature, $H_{C2}(T)$, the shift in T_C in different applied magnetic fields was determined from magnetization and resistivity data. Resistivity measurement as a function of temperature, $\rho(T)$, was performed at different applied magnetic fields up to 0.36 T (see the inset of Fig. 4). Figure 4 displays the linear variation of $H_{C2}(T)$ when plotted against the reduced temperature
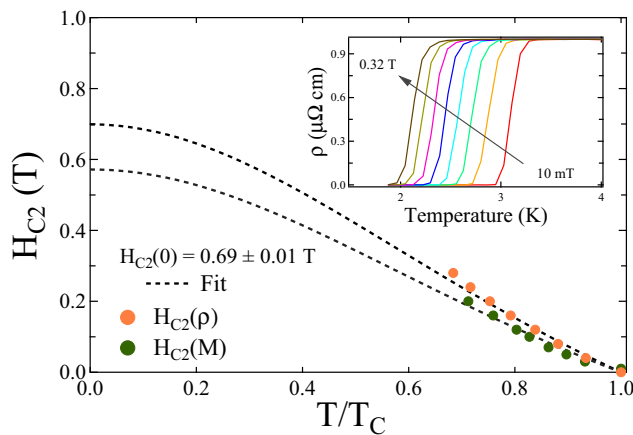

FIG. 4. Temperature dependence of the upper critical field H_{C2} determined via magnetization and resistivity measurements. The solid lines are fit to the data using Eq. (5). The inset shows the resistivity curves at different applied magnetic fields.

$t = T/T_C$. Both resistivity and magnetization are in good agreement with the Ginzburg-Landau (GL) relation,

$$H_{C2}(T) = H_{C2}(0)\left[\frac{(1-t^2)}{(1+t^2)}\right]. \quad (5)$$

The value obtained after fitting Eq. (5) is $H_{C2}(0) = 0.69 \pm 0.01$ T.

The orbital limiting field $H_{C2}^{\mathrm{orbital}}(0)$ is the field where the Cooper pairs break due to an increased kinetic energy, and it is given by the Werthamar-Helfand-Hohenberg (WHH) expression [41,42]

$$H_{C2}^{\mathrm{orbital}}(0) = -\alpha T_C \left.\frac{dH_{C2}(T)}{dT}\right|_{T=T_C}, \quad (6)$$

where α is the purity factor given by 0.693 and 0.73 for superconductors in the dirty and clean limit, respectively. The initial slope $\frac{-dH_{C2}(T)}{dT}$ in the vicinity of $T = T_C$ yields a value of 0.67 ± 0.04 T/K, which gives $H_{C2}^{\mathrm{orbital}}(0) = 1.41 \pm 0.08$ T. Another mechanism that suppresses superconductivity is the Pauli-limiting field. According to the BCS theory, the Pauli-limiting field is given by $H_{C2}^{P}(0) = 1.86T_C$, which for $T_C = 3.05 \pm 0.05$ K produces $H_{C2}^{P}(0) = 5.7 \pm 0.1$ T. The Maki parameter, which measures the relative strengths of the orbital and Pauli-limiting fields, was calculated using $\alpha_M = \sqrt{2}H_{C2}^{\mathrm{orb}}(0)/H_{C2}^{P}(0) = 0.16 \pm 0.01$. Such a small value of the Maki parameter implies that the effect of the Pauli limiting field is negligible.

The characteristic Ginzburg-Landau coherence length ξ_{GL} can be evaluated using the $H_{C2}(0)$ value from the relation [43]

$$H_{C2}(0) = \frac{\Phi_0}{2\pi\xi_{\mathrm{GL}}^2}, \quad (7)$$

where ϕ_0 ($= 2.07 \times 10^{-15}$ T m^2) is the magnetic flux quantum. Using $H_{C2}(0) = 0.69 \pm 0.01$ T, we estimated $\xi_{\mathrm{GL}}(0) = 218 \pm 4$ Å. The Ginzburg-Landau penetration depth $\lambda_{\mathrm{GL}}(0)$ can be calculated from the relation

$$H_{C1}(0) = \frac{\Phi_0}{4\pi\lambda_{\mathrm{GL}}^2(0)}\left(\ln\frac{\lambda_{\mathrm{GL}}(0)}{\xi_{\mathrm{GL}}(0)} + 0.12\right). \quad (8)$$
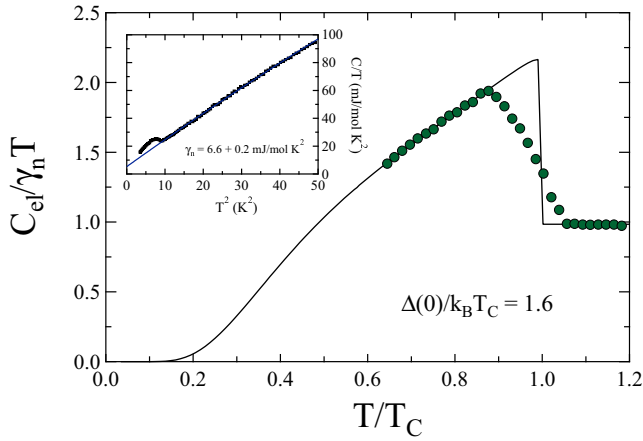
FIG. 5. Temperature dependence of electronic specific-heat fitting with the isotropic BCS expression [Eq. (17)]. The inset shows the C/T vs T^2 data fit to Eq. (10).

Using the values of $H_{C1}(0) = 2.1 \pm 0.2$ mT and $\xi_{GL}(0) = 218 \pm 4$ Å, we calculated $\lambda_{GL}(0) = 5047 \pm 28$ Å. The Ginzburg-Landau parameter for the sample is calculated with the equation

$$\kappa_{GL} = \frac{\lambda_{GL}(0)}{\xi_{GL}(0)}. \tag{9}$$

This yields a value of $\kappa_{GL} = 23 \pm 1$. For a type-II superconductor, $\kappa_{GL} \geqslant \frac{1}{\sqrt{2}}$. Therefore, it is clear that LaPtGe is a type-II superconductor. The thermodynamic critical field H_C can be calculated using the relation $H_{C1}(0)H_{C2}(0) = H_C^2 \ln \kappa_{GL}$, giving the value as $H_C = 21 \pm 1$ mT.

3. Specific heat

Specific-heat data were collected in the temperature range $1.9 \leqslant T \leqslant 300$ K. The bulk nature of the superconducting state is evidenced by the occurrence of a well-developed discontinuity at $T_C = 2.9 \pm 0.05$ K. The normal-state specific-heat data can be extracted by the relation

$$\frac{C}{T} = \gamma_n + \beta_3 T^2 + \beta_5 T^4. \tag{10}$$

This represents the contribution from the electronic as well as the phononic origin to the total specific heat. Fitting the above equation in the data above T_C determines the Sommerfeld coefficient (γ_n), which describes the electronic contribution, the Debye constant (β_3) representing the phononic contribution, and β_5 representing the anharmonic contribution. The solid blue line in the inset of Fig. 5 in the normal-state region ($10 \leqslant T^2 \leqslant 60$ K) represents the best fit to the data, which yields $\gamma_n = 6.6 \pm 0.2$ mJ/mol K^2, $\beta_3 = 1.83 \pm 0.01$ mJ/mol K^4, and $\beta_5 = 0.000\,49 \pm 0.000\,02$ mJ/mol K^6. The Debye temperature θ_D can be estimated with the relation [21]

$$\theta_D = \left(\frac{12\pi^4 R N}{5\beta_3} \right)^{\frac{1}{3}}, \tag{11}$$

Here $R = 8.314$ j mol^{-1} K^{-1} is the universal gas constant and N (= 3) is the number of atoms per formula unit. The estimated value of $\theta_D = 147 \pm 4$ K is consistent with the

value obtained from the parallel-resistor model. Under the assumption of a degenerate electron gas of noninteracting particles, the Sommerfeld coefficient γ_n is proportional to the density of states at the Fermi level. The value of γ_n can be used to estimate the density of states at the Fermi level $D_C(E_F)$ via the relation

$$\gamma_n = \left(\frac{\pi^2 k_B^2}{3} \right) D_C(E_F), \tag{12}$$

where k_B is Boltzmann's constant. Substituting $\gamma_n = 6.6 \pm 0.2$ mJ/mol K^2 yields $D_C(E_F) = 2.8 \pm 0.1$ $\frac{\text{states}}{\text{eV f.u.}}$. The electron-phonon coupling constant $\lambda_{e\text{-ph}}$, a dimensionless number that describes the coupling between the electron and the phonon, is given by McMillan's equation [44],

$$\lambda_{e\text{-ph}} = \frac{1.04 + \mu^* \ln(\theta_D/1.45T_C)}{(1 - 0.62\mu^*)\ln(\theta_D/1.45T_C) - 1.04}, \tag{13}$$

where μ^* is the repulsive screened Coulomb potential having typical material specific values in the range $0.1 \leqslant \mu^* \leqslant 0.15$, where 0.13 is used for intermetallic superconductors. Incorporating the values of θ_D and T_C yields $\lambda_{e\text{-ph}} = 0.67 \pm 0.03$, which is comparable to those in noncentrosymmetric superconductors such as 0.63 in Re$_6$Hf [20] and 0.5 for LaRhSi$_3$ [45] indicating that the electron-phonon coupling is moderately strong in LaPtGe. The bare band-structure density of states $D_{\text{band}}(E_F)$ and m^*_{band} are related to $D_C(E_F)$ by the relations

$$D_C(E_F) = D_{\text{band}}(E_F)(1 + \lambda_{e\text{-ph}}), \tag{14}$$

$$m^* = m^*_{\text{band}}(1 + \lambda_{e\text{-ph}}). \tag{15}$$

Using the value of $\lambda_{e\text{-ph}} = 0.67$ in Eqs. (14) and (15) yields $D_{\text{band}}(E_F) = 1.7 \pm 0.1$ $\frac{\text{states}}{\text{eV f.u.}}$ and the effective mass of quasiparticle as $1.67m_e$, where we used $m^*_{\text{band}} = m_e$. The condensation energy $U(0)$, which is the difference between the ground-state energies of the normal state and the superconducting state, can be estimated using the relation $U(0) = \frac{1}{2}\Delta^2(0)D_{\text{band}}(E_F)$ employing $\Delta^2(0) = 4.1 \times 10^{-45}$ J and $D_{\text{band}}(E_F) = 1.1378 \times 10^{43}$ J^{-1} mol^{-1} from specific-heat measurements to give $U(0) = 23.2 \pm 0.4$ mJ/mol.

The electronic contribution to the specific heat, $C_{\text{el}}(T)$, is calculated by subtracting the phononic contribution of the specific heat from the total specific heat $C(T)$. The specific-heat jump $\frac{\Delta C_{\text{el}}}{T_C}$ at T_C is 7.72 ± 0.05 mJ/mol K^2. The normalized jump in specific heat is then obtained as $\frac{\Delta C_{\text{el}}}{\gamma_n T_C} = 1.17 \pm 0.06$, which is lower than the BCS value 1.43. Similar low values have also been reported for isostructural compounds [46]. The temperature dependence of the specific heat in the superconducting state can be best described by a single-gap BCS expression for normalized entropy, S,

$$\frac{S}{\gamma_n T_C} = -\frac{6}{\pi^2} \left(\frac{\Delta(0)}{k_B T_C} \right) \int_0^\infty [f \ln(f) + (1-f)\ln(1-f)]dy, \tag{16}$$

where $f(\xi) = \{\exp[E(\xi)/k_B T] + 1\}^{-1}$ is the Fermi function, $E(\xi) = \sqrt{\xi^2 + \Delta^2(t)}$, where $E(\xi)$ is the energy of the normal electrons measured relative to the Fermi energy, $y = \xi/\Delta(0)$, $t = T/T_C$, and $\Delta(t) = \tanh(1.82\{1.018[(1/t) - 1]\}^{0.51})$ is the
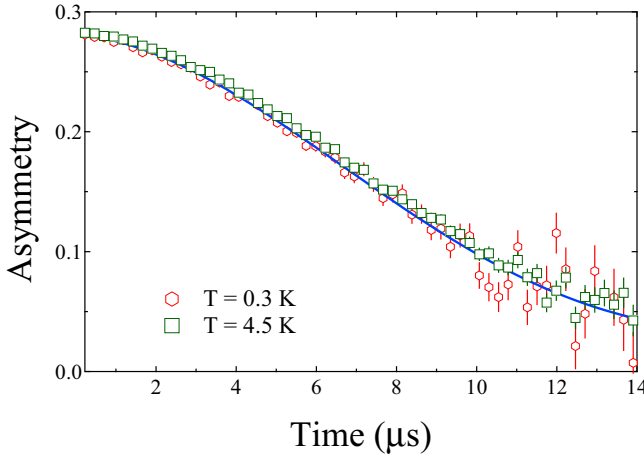
FIG. 6. ZF-μSR spectra collected above ($T = 4.5$ K) and below ($T = 0.3$ K) the transition temperature. The solid line is a fit to Eq. (19).
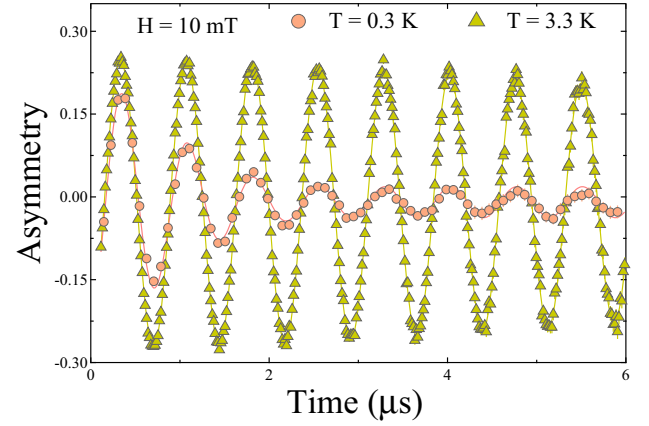

FIG. 7. TF-μSR signals collected above ($T = 3.3$ K) and below ($T = 0.3$ K) the transition temperature in an applied transverse magnetic field of 10 mT. Fast decay of the signal below T_C indicates the vortex formation.

BCS approximation for the temperature dependence of the energy gap. The normalized electronic specific heat is related to the normalized entropy by

$$\frac{C_{\text{el}}}{\gamma_n T_C} = t \frac{d(S/\gamma_n T_C)}{dt}, \tag{17}$$

where C_{el} below T_C is described by the above equation, whereas above T_C it is equal to $\gamma_n T_C$. Figure 5 shows the fitting of the specific-heat data using Eq. (17). Fitting yields a value $\alpha = \Delta(0)/k_B T_C = 1.6 \pm 0.1$, which is slightly less than the BCS value $\alpha = 1.76$.

4. Muon spin relaxation and rotation

Further analysis of the superconducting ground state of LaPtGe was carried out by muon spin rotation and relaxation (μSR) measurements. Zero-field muon spin relaxation spectra (ZF-μSR) collected at temperatures above and below T_C are shown in Fig. 6. The absence of any atomic moments associated with the magnetic structure was confirmed by the nonoscillatory nature of the spectrum within the time window of μSR. The depolarization in such cases is accounted for by the presence of static, randomly oriented nuclear moments. In the absence of atomic moments, muon spin relaxation in zero field is given by the Gaussian Kubo-Toyabe (KT) function [47]

$$G_{\text{KT}}(t) = \frac{1}{3} + \frac{2}{3}(1 - \sigma_{\text{ZF}}^2 t^2) \exp\left(\frac{-\sigma_{\text{ZF}}^2 t^2}{2}\right), \tag{18}$$

where σ_{ZF} is the relaxation due to static, randomly oriented local fields associated with the nuclear moments at the muon site. The spectra can be well described by the function

$$A(t) = A_1 G_{\text{KT}}(t) \exp(-\Lambda t) + A_{\text{BG}}, \tag{19}$$

where A_1 corresponds to the initial asymmetry, Λ is the electronic relaxation rate, which fluctuates on a timescale much faster than the muon timescale, and A_{BG} is the time-dependent background contribution from the muons stopped in the sample holder. The temperature dependence of the fit parameters Λ and σ showed no perceptible temperature

dependence above and below T_C, indicating that time-reversal symmetry is preserved within the detection limit of μSR for LaPtGe.

Transverse field muon spin rotation experiments (TF-μSR) were performed in an applied field of 10 mT. Figure 7 shows the spectra collected above and below T_C. The enhanced depolarization rate below T_C is due to the field distribution, formed by the flux line lattice in the mixed state of the superconductor. Assuming the hexagonal vortex lattice for LaPtGe, the TF-μSR precession signal is well described by the oscillatory decaying Gaussian function

$$G_{\text{TF}}(t) = A_1 \exp\left(\frac{-\sigma_{\text{TF}}^2 t^2}{2}\right) \cos(w_1 t + \phi) + A_2 \cos(w_2 t + \phi), \tag{20}$$

where ω_1 and ω_2 are the frequencies of the muon precession signal and background, respectively, ϕ is the initial phase offset, and σ_{TF} is the Gaussian muon spin depolarization rate. The value of σ_{TF} depends on the distribution of vortices in the superconducting state, which causes an increase in depolarization below T_C. $\sigma_{\text{TF}}(T)$ at different applied fields in the range $10 \leqslant H \leqslant 40$ mT was extracted using Eq. (20) as shown in Fig. 8(a). The temperature-independent depolarization due to static fields arising from the nuclear magnetic moments σ_N adds in quadrature to the contribution from the field variation across the flux line lattice σ_{FLL},

$$\sigma_{\text{TF}}^2 = \sigma_N^2 + \sigma_{\text{FLL}}^2. \tag{21}$$

The field dependence of the depolarization rate $\sigma(H)$ was determined by making isothermal cuts to the $\sigma_{\text{TF}}(T)$ and is shown in Fig. 8(b). According to Ginzburg-Landau theory, which explains the Abrikosov hexagonal lattice in a type-II superconductor, the magnetic penetration depth λ is related to σ_{FLL} by [48]

$$\sigma_{\text{FLL}} \, (\mu s^{-1}) = 4.854 \times 10^4 (1 - h)[1 + 1.21(1 - \sqrt{h})^3]$$
$$\times \lambda^{-2} \, (\text{nm}^{-2}), \tag{22}$$

where $h = H/H_{C2}$ is the reduced field and ϕ_0 is the magnetic flux quantum. The resulting fits to the data are shown as solid
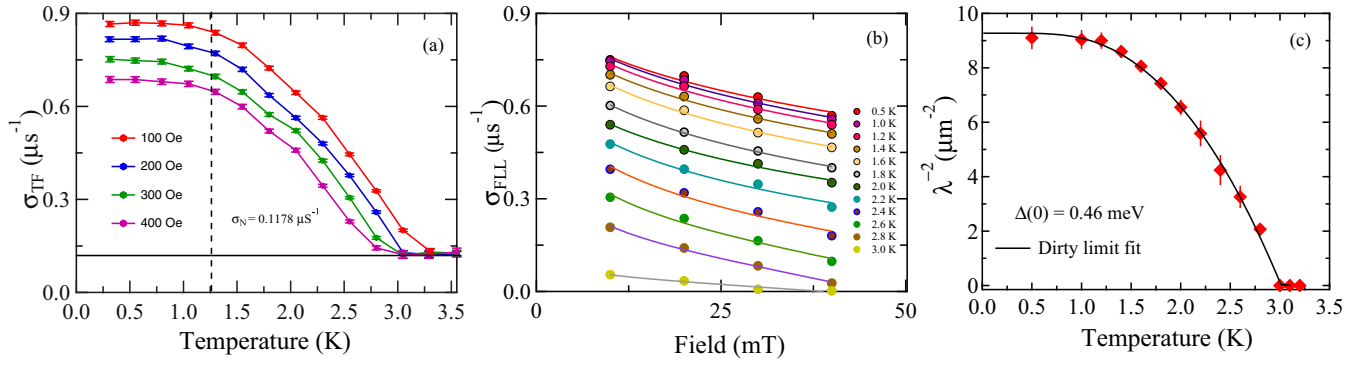
FIG. 8. (a) Temperature dependence of the TF-μSR depolarization rate collected at different fields. (b) Isothermal field dependence of depolarization. (c) Temperature dependence of inverse magnetic penetration depth square. The solid line is the fit to the s-wave model.

lines in Fig. 8(b). The estimated value of H_{C2} obtained using Eq. (22) (not shown here) is consistent with the resistivity and magnetization measurements. The temperature dependence of λ^{-2} is shown in Fig. 8(c), where λ^{-2} is assumed to be zero above T_C. The data show a characteristic plateau at low temperature followed by a decrease as temperature increases. The temperature dependence of the superfluid density can be calculated for an isotropic s-wave superconductor in the dirty limit using the expression

$$\frac{\lambda^{-2}(T)}{\lambda^{-2}(0)} = \frac{\Delta(T)}{\Delta(0)} \tanh\left[\frac{\Delta(T)}{2k_B T}\right], \qquad (23)$$

where $\Delta(T) = \Delta_0 \tanh(1.82\{1.018[(T_C/T) - 1]\}^{0.51})$ is the BCS approximation for the temperature dependence of the energy gap. The solid lines in Fig. 8(c) are a result of the fit to this model for the values of $\lambda^{-2}(T)$. The fit yields a value of the energy gap as $\Delta_0 = 0.46 \pm 0.01$ meV, which gives the BCS parameter $\Delta_0/k_B T_C = 1.79 \pm 0.07$, which is very close to the BCS value of 1.76 implying the moderately coupled nature of the sample. The specific-heat measurement also suggested the moderately coupled superelectrons, where $\Delta_0/k_B T_C = 1.6 \pm 0.1$. A slight difference in the energy gap value is due to the microscopic and macroscopic nature of μSR and specific heat, respectively. So the specific-heat measurement along with the TF-μSR results confirm that LaPtGe is an s-wave superconductor.

The quasiparticle number density per unit volume and mean free path is related to the Sommerfeld coefficient via the relation [49]

$$\gamma_n = \left(\frac{\pi}{3}\right)^{2/3} \frac{k_B^2 m^* V_{\text{f.u.}} n^{1/3}}{\hbar^2 N_A}, \qquad (24)$$

where k_B is the Boltzmann constant, N_A is the Avogadro number, $V_{\text{f.u.}}$ is the volume of a formula unit, and m^* is the effective mass of quasiparticles. The electronic mean free path l and Fermi velocity v_F are correlated with residual resistivity by the relation

$$l = \frac{3\pi^2 \hbar^3}{e^2 \rho_0 m^{*2} v_F^2} \qquad (25)$$

while the Fermi velocity v_F can be written in terms of the effective mass and the carrier density by

$$n = \frac{1}{3\pi^2}\left(\frac{m^* v_f}{\hbar}\right)^3. \qquad (26)$$

The dirty limit expression for the penetration depth $\lambda_{\text{GL}}(0)$ is given by

$$\lambda_{\text{GL}}(0) = \lambda_L \left(1 + \frac{\xi_0}{l}\right)^{1/2}, \qquad (27)$$

where ξ_0 is the BCS coherence length. The London penetration depth λ_L is given by

$$\lambda_L = \left(\frac{m^*}{\mu_0 n e^2}\right)^{1/2}. \qquad (28)$$

The BCS coherence length ξ_0 and the Ginzburg-Landau coherence $\xi_{\text{GL}}(0)$ at $T = 0$ K in the dirty limit is related by the expression

$$\frac{\xi_{\text{GL}}(0)}{\xi_0} = \frac{\pi}{2\sqrt{3}}\left(1 + \frac{\xi_0}{l}\right)^{-1/2}. \qquad (29)$$

Equations (24)–(29) form a system of four equations that can be used to estimate the parameters m^*, n, l, and ξ_0 as done in Ref. [39]. The system of equations was solved simultaneously using the values $\gamma_n = 6.6 \pm 0.2$ mJ mol^{-1} K^{-2},

TABLE I. Superconducting and normal-state parameters of LaPtGe.

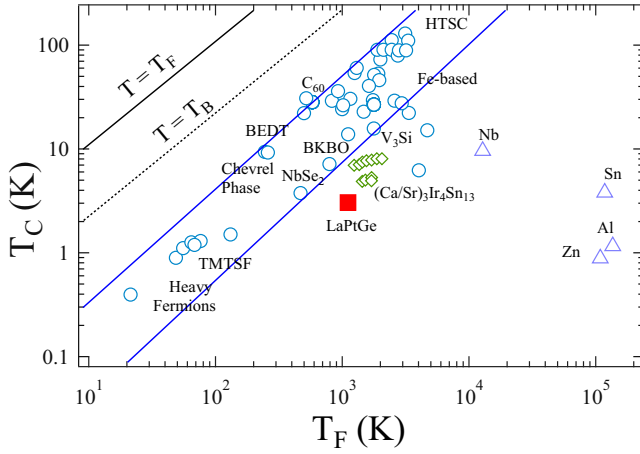| Parameters	Unit	LaPtGe
T_C	K	3.05
$H_{C1}(0)$	mT	2.1
$H_{C2}(0)$	T	0.69
$H_{C2}^P(0)$	T	5.67
ξ_{GL}	Å	218
λ_{GL}	Å	5047
k_{GL}		23
$\Delta C_{\text{el}}/\gamma_n T_C$		1.17
$\Delta(0)/k_B T_C$		1.6
m^*/m_e		7.08
n	10^{27} m^{-3}	2.7
l	Å	23.84
ξ_0	Å	59
ξ_0/l		2.47
v_f	10^4 ms^{-1}	6.63
λ_L	Å	2721
T_C/T_F		0.0026

FIG. 9. The Uemura plot showing the superconducting transition temperature T_c vs the effective Fermi temperature T_F, where LaPtGe is shown as a solid red marker. Other data points plotted between the blue solid lines are the different families of unconventional superconductors [50,51].

$\xi_{GL}(0) = 218 \pm 4$ Å, and $\rho_0 = 253 \pm 2$ $\mu\Omega$ cm. The estimated values are tabulated in Table I. It is clear that $\xi_0 > l$, indicating that LaPtGe is in the dirty limit. The estimated value of mean free path l is of the same order as observed in other noncentrosymmetric superconductors, where dirty limit superconductivity was observed [39,52,53].

For a 3D system, the Fermi temperature T_F is given by the relation

$$k_B T_F = \frac{\hbar^2}{2}(3\pi^2)^{2/3}\frac{n^{2/3}}{m^*}, \qquad (30)$$

where n is the quasiparticle number density per unit volume.

According to Uemura *et al.* [54], superconductors can be conveniently classified according to their $\frac{T_C}{T_F}$ ratio. It was shown that for unconventional superconductors this ratio falls in the range $0.01 \leqslant \frac{T_C}{T_F} \leqslant 0.1$.

Using the estimated value of n in Eq. (30) we get $T_F = 1158$ K, giving $\frac{T_C}{T_F} = 0.0026$, which places LaPtGe away from the unconventional superconductors as shown by a solid red symbol in Fig. 9, where solid blue lines represent the band of unconventional superconductors.

IV. CONCLUSION

High-purity samples of LaPtGe are prepared by arc-melting. X-ray diffraction confirms that the sample crystallized in a noncentrosymmetric LaPtSi structure (space group no. 109). The sample exhibited superconductivity with a transition temperature $T_C = 3.05 \pm 0.05$ K. Comprehensive transport, magnetization, and heat-capacity measurements suggest that LaPtGe is a moderately coupled *s*-wave superconductor. Transverse field muon experiments further confirm that it is a moderately coupled *s*-wave superconductor. Zero-field μSR measurements did not find any evidence of time-reversal symmetry breaking in the superconducting ground state. The above-mentioned results suggest that the antisymmetric spin-orbital coupling does not affect the superconducting ground state. It is clearly important to work on more noncentrosymmetric superconductors with high antisymmetric spin-orbital coupling to understand the complex superconducting ground state of these superconductors.

[1] J. Bardeen, L. N. Cooper, and J. R. Schrieffer, Phys. Rev. **108**, 1175 (1957).

[2] E. Bauer, G. Rogl, X.-Q. Chen, R. T. Khan, H. Michor, G. Hilscher, E. Royanian, K. Kumagai, D. Z. Li, Y. Y. Li, R. Podloucky, and P. Rogl, Phys. Rev. B **82**, 064511 (2010).

[3] S. Chadov, X. Qi, J. Kbler, G. H. Fecher, C. Felser, and S. C. Zhang, Nat. Mater. **9**, 541 (2010).

[4] M. Z. Hasan and C. L. Kane, Rev. Mod. Phys. **82**, 3045 (2010).

[5] C. K. Lu and S. Yip, Phys. Rev. B **82**, 104501 (2010).

[6] E. Bauer and M. Sigrist, *Non-centrosymmetric Superconductor: Introduction and Overview* (Springer-Verlag, Heidelberg, 2012).

[7] L. P. Gor'kov and E. I. Rashba, Phys. Rev. Lett. **87**, 037004 (2001).

[8] S. K. Yip, Phys. Rev. B **65**, 144508 (2002).

[9] K. V. Samokhin, E. S. Zijlstra, and S. K. Bose, Phys. Rev. B **69**, 094514 (2004).

[10] I. A. Sergienko and S. H. Curnoe, Phys. Rev. B **70**, 214510 (2004).

[11] P. A. Frigeri, D. F. Agterberg, A. Koga, and M. Sigrist, Phys. Rev. Lett. **92**, 097001 (2004).

[12] S. Fujimoto, Phys. Rev. B **72**, 024515 (2005).

[13] S. Fujimoto, J. Phys. Soc. Jpn. **75**, 083704 (2006).

[14] S. Fujimoto, J. Phys. Soc. Jpn. **76**, 051008 (2007).

[15] M. Sigrist, D. F. Agterberg, P. A. Frigeri, N. Hayashi, R. P. Kaur, A. Koga, I. Milat, K. Wakabayashi, and Y. Yanase, J. Magn. Magn. Mater. **310**, 536 (2007).

[16] S. Harada, J. J. Zhou, Y. G. Yao, Y. Inada, and G.-Q. Zheng, Phys. Rev. B **86**, 220502(R) (2012).

[17] E. Bauer, G. Hilscher, H. Michor, Ch. Paul, E. W. Scheidt, A. Gribanov, Yu. Seropegin, H. Noël, M. Sigrist, and P. Rogl, Phys. Rev. Lett. **92**, 027003 (2004).

[18] M. A. Khan, A. B. Karki, T. Samanta, D. Browne, S. Stadler, I. Vekhter, A. Pandey, P. W. Adams, D. P. Young, S. Teknowijoyo, K. Cho, R. Prozorov, and D. E. Graf, Phys. Rev. B **94**, 144515 (2016).

[19] R. P. Singh, A. D. Hillier, B. Mazidian, J. Quintanilla, J. F. Annett, D. McK. Paul, G. Balakrishnan, and M. R. Lees, Phys. Rev. Lett. **112**, 107002 (2014).

[20] D. Singh, A. D. Hillier, A. Thamizhavel, and R. P. Singh, Phys. Rev. B **94**, 054515 (2016).

[21] D. Singh, J. A. T. Barker, A. Thamizhavel, D. McK. Paul, A. D. Hillier, and R. P. Singh, Phys. Rev. B **96**, 180501(R) (2017).

[22] D. Singh, K. P. Sajilesh, J. A. T. Barker, D. M. Paul, A. D. Hillier, and R. P. Singh, Phys. Rev. B **97**, 100505(R) (2018).

[23] B. Chen, Y. Guo, H. Wang, Q. Su, Q. Mao, J. Du, Y. Zhou, J. Yang, and M. Fang, Phys. Rev. B **94**, 024518 (2016).

[24] T. Akazawa, H. Hidaka, H. Kotegawa, T. C. Kobayashi, T. Fujiwara, E. Yamamoto, Y. Haga, R. Settai, and Y. Ōnuki, J. Phys. Soc. Jpn. **73**, 3129 (2004).

[25] A. D. Hillier, J. Quintanilla, and R. Cywinski, Phys. Rev. Lett. **102**, 117007 (2009).

[26] K. Togano, P. Badica, Y. Nakamori, S. Orimo, H. Takeya, and K. Hirata, Phys. Rev. Lett. **93**, 247004 (2004).

[27] J. A. T. Barker, D. Singh, A. Thamizhavel, A. D. Hillier, M. R. Lees, G. Balakrishnan, D McK. Paul, and R. P. Singh, Phys. Rev. Lett. **115**, 267001 (2015).

[28] G. M. Luke, Y. Fudamoto, K. M. Kojima, M. I. Larkin, J. Merrin, B. Nachumi, Y. J. Uemura, Y. Maeno, Z. Q. Mao, Y. Mori, H. Nakamura, and M. Sigrist, Nature (London) **394**, 558 (1998)

[29] G. M. Luke, A. Keren, L. P. Le, W. D. Wu, Y. J. Uemura, D. A. Bonn, L. Taillefer, and J. D. Garrett, Phys. Rev. Lett. **71**, 1466 (1993).

[30] R. H. Heffner, J. L. Smith, J. O. Willis, P. Birrer, C. Baines, F. N. Gygax, B. Hitti, E. Lippelt, H. R. Ott, A. Schenck, E. A. Knetsch, J. A. Mydosh, and D. E. MacLaughlin, Phys. Rev. Lett. **65**, 2816 (1990).

[31] Y. Aoki, A. Tsuchiya, T. Kanayama, S. R. Saha, H. Sugawara, H. Sato, W. Higemoto, A. Koda, K. Ohishi, K. Nishiyama, and R. Kadono, Phys. Rev. Lett. **91**, 067003 (2003).

[32] P. K. Biswas, H. Luetkens, T. Neupert, T. Stürzer, C. Baines, G. Pascua, A. P. Schnyder, M. H. Fischer, J. Goryo, M. R. Lees, H. Maeter, F. Brückner, H.-H. Klauss, M. Nicklas, P. J. Baker, A. D. Hillier, M. Sigrist, A. Amato, and D. Johrendt, Phys. Rev. B **87**, 180503 (2013).

[33] J. Evers, G. Oehlinger, and A. Weiss, Solid State Commun. **50**, 61 (1984).

[34] S. Palazzese, J. F. Landaeta, D. Subero, E. Bauer, and I. Bonalde, J. Phys.: Condens. Matter **30**, 255603 (2018).

[35] F. Kneidinger, H. Michor, A. Sidorenko, E. Bauer, I. Zeiringer, P. Rogl, C. Blaas-Schenner, D. Reith, and R. Podloucky, Phys. Rev. B **88**, 104508 (2013).

[36] H. Wiesmann, M. Gurvitch, H. Lutz, A. K. Ghosh, B. Schwarz, M. Strongin, P. B. Allen, and J. W. Halley, Phys. Rev. Lett. **38**, 782 (1977).

[37] Z. Fisk and G. W. Webb, Phys. Rev. Lett. **36**, 1084 (1976).

[38] O. Gunnarsson, M. Calandra, and J. E. Han, Rev. Mod. Phys. **75**, 1085 (2003).

[39] D. A. Mayoh, J. A. T. Barker, R. P. Singh, G. Balakrishnan, D. McK. Paul, and M. R. Lees, Phys. Rev. B **96**, 064521 (2017).

[40] G. Grimvall, *The Electron-Phonon Interaction in Metals* (North-Holland, Amsterdam, 1981).

[41] E. Helfand and N. R. Werthamer, Phys. Rev. **147**, 288 (1966).

[42] N. R. Werthamer, E. Helfand, and P. C. Hohenberg, Phys. Rev. **147**, 295 (1966).

[43] M. Tinkham, *Introduction to Superconductivity*, 2nd ed. (McGraw-Hill, New York, 1996).

[44] W. L. McMillan, Phys. Rev. **167**, 331 (1968).

[45] V. K. Anand, A. D. Hillier, D. T. Adroja, A. M. Strydom, H. Michor, K. A. McEwen, and B. D. Rainford, Phys. Rev. B **83**, 064522 (2011).

[46] Y. Qi, J. Guo, H. Lei, Z. Xiao, T. Kamiya, and H. Hosono, Phys. Rev. B **89**, 024517 (2014).

[47] R. S. Hayano, Y. J. Uemura, J. Imazato, N. Nishida, T. Yamazaki, and R. Kubo, Phys. Rev. B **20**, 850 (1979).

[48] E. H. Brandt, Phys. Rev. B **68**, 054506 (2003).

[49] C. Kittel, *Introduction to Solid State Physics*, 8th ed. (Wiley, New York, 2005).

[50] K. Hashimoto, K. Cho, T. Shibauchi, S. Kasahara, Y. Mizukami, R. Katsumata, Y. Tsuruhara, T. Terashima, H. Ikeda, M. A. Tanatar, H. Kitano, N. Salovich, R. W. Giannetta, P. Walmsley, A. Carrington, R. Prozorov, and Y. Matsuda, Science **336**, 1554 (2012).

[51] R. Khasanov, H. Luetkens, A. Amato, H. H. Klauss, Z. A. Ren, J. Yang, W. Lu, and Z. X. Zhao, Phys. Rev. B **78**, 092506 (2008).

[52] C. Cirillo, R. Fittipaldi, M. Smidman, G. Carapella, C. Attanasio, A. Vecchione, R. P. Singh, M. R. Lees, G. Balakrishnan, and M. Cuoco, Phys. Rev. B **91**, 134508 (2015).

[53] P. K. Biswas, M. R. Lees, A. D. Hillier, R. I. Smith, W. G. Marshall, and D. McK. Paul, Phys. Rev. B **84**, 184529 (2011).

[54] Y. J. Uemura, G. M. Luke, B. J. Sternlieb, J. H. Brewer, J. F. Carolan, W. N. Hardy, R. Kadono, J. R. Kempton, R. F. Kiefl, S. R. Kreitzman, P. Mulhern, T. M. Riseman, D. L. Williams, B. X. Yang, S. Uchida, H. Takagi, J. Gopalakrishnan, A. W. Sleight, M. A. Subramanian, C. L. Chien, M. Z. Cieplak, G. Xiao, V. Y. Lee, B. W. Statt, C. E. Stronach, W. J. Kossler, and X. H. Yu, Phys. Rev. Lett. **62**, 2317 (1989).